Neutron powder diffraction study of rhombohedral rare-earth aluminates and the rhombohedral to cubic phase transition



2000 J. Phys.: Condens. Matter 12 349

(http://iopscience.iop.org/0953-8984/12/4/301)

J. Phys.: Condens. Matter **12** (2000) 349–365. Printed in the UK PII: S0953-8984(00)06437-7

# Neutron powder diffraction study of rhombohedral rare-earth aluminates and the rhombohedral to cubic phase transition

Christopher J Howard†§, Brendan J Kennedy† and Bryan C Chakoumakos‡

† School of Chemistry, The University of Sydney, Sydney NSW 2006, Australia
‡ Solid State Division, Oak Ridge National Laboratory, Oak Ridge, TN 37831, USA

Received 28 July 1999, in final form 10 November 1999

**Abstract.** Neutron powder diffraction has been used to examine the structural changes of the rare-earth aluminates $LaAlO_3$, $PrAlO_3$ and $NdAlO_3$ over a wide range of temperatures. At room temperature, all three aluminates adopt the rhombohedral perovskite structure in space group $R\bar{3}c$ ($a = 5.3647(1)$ Å, $c = 13.1114(3)$ Å for $LaAlO_3$, $a = 5.3337(2)$ Å, $c = 12.9842(4)$ Å for $PrAlO_3$, $a = 5.3223(2)$ Å, $c = 12.9292(5)$ Å for $NdAlO_3$). The rhombohedral structure is characterized by rotation of the oxygen atom octahedra about the threefold axis, and compression of these octahedra parallel to the same axis. As the temperature is increased, the rotation angle and the compression decrease, indicative of an approach to the cubic symmetry of the ideal perovskite. Only for $LaAlO_3$, however, was the transition at a low enough temperature to unequivocally obtain the cubic phase. For $PrAlO_3$ the transition was closely approached before the sample can failed, but for $NdAlO_3$ the transition appeared to be inaccessible within the available temperature range. The rotation angle is taken to represent the order parameter, and its temperature variation is well described by a generalized mean field approach. Such a description suggests the transitions are continuous, being at 820 K and second order for the transition in $LaAlO_3$, and at 1768 K and tricritical for the transition in $PrAlO_3$. In the proximity of the phase transition, the octahedral compression varies with the square of the rotation angle, though this description is inadequate remote from the transition, and the constant of proportionality is different for the different compounds.

## 1. Introduction

As part of current systematic studies of compounds of the perovskite family, with particular emphasis on structural phase transitions [1–7], we have used neutron powder diffraction methods to investigate the crystal structures of rhombohedral ($R\bar{3}c$) or cubic ($Pm\bar{3}m$) $LaAlO_3$, $PrAlO_3$ and $NdAlO_3$, and their evolution to temperatures as high as 1763 K. The study of the rare earth aluminates follows our recent study [5] of the closely related gallate $LaGaO_3$. This gallate is orthorhombic in space group $Pbnm$ at ambient temperature, and undergoes a first order transition to rhombohedral, space group $R\bar{3}c$, at 418 K [5, 8–10]. A major aim of the measurements on $LaGaO_3$ was to study the possibly continuous transition [2] from the rhombohedral to cubic structure. Though the angle of rotation of the oxygen atom octahedra and the strain of these octahedra both decreased with temperature, even at the maximum temperature of the measurements (1673 K), which was close to the maximum accessible temperature in the furnace used, the transition to cubic still seemed well out of reach. The rare-earth aluminates were chosen for their potential to show the transition from rhombohedral

§ On leave from Australian Nuclear Science and Technology Organization, Private Mail Bag 1, Menai, NSW 2234, Australia.

0953-8984/00/040349+17$30.00  

to cubic phase at lower temperatures, within a readily accessible temperature range, so that detailed investigations of the rhombohedral–cubic phase transition might be possible.

The first significant study of the rhombohedral rare earth aluminates was an x-ray diffraction study, using single crystal and powder techniques, by Geller and Bala [11]. Optical microscopy was also employed. It was established that the crystal structures of $LaAlO_3$, $PrAlO_3$ and $NdAlO_3$ were all rhombohedral at room temperature, and the lattice parameters were reported for all three compounds. Powder x-ray diffraction patterns from $LaAlO_3$ and $PrAlO_3$ were recorded (on film) at elevated temperatures, and from these it was observed that $LaAlO_3$ undergoes a transition to the cubic phase at a few hundreds of degrees celsius, whereas $PrAlO_3$ remains rhombohedral to the highest temperature achieved (1220 K). The presently accepted space group for the rhombohedral structures, $R\bar{3}c$, was suggested in an early x-ray and neutron diffraction study of $LaAlO_3$ at room temperature [12], and more definitively by evidence from nuclear quadrupole resonance that all Al atoms are equivalent [13]. The rhombohedral to cubic phase transition in $LaAlO_3$ subsequently attracted considerable attention [8, 14–19]. The most informative investigation, from a structural point of view [15], comprised electron paramagnetic resonance measurements on a monodomain crystal of $LaAlO_3$ having 0.02% $Fe^{3+}$ on the $Al^{3+}$ site. The data were analysed to show the angle of rotation of the oxygen octahedron as a function of temperature, from liquid helium temperatures through to the phase transition, estimated to occur at $800 \pm 10$ K. It was suggested that the rotation angle could be taken to represent the order parameter and, from the variation of this angle with temperature, that the transition was second order. Inelastic neutron scattering [17] and Raman spectroscopy [18] show soft modes associated with the transition. Recently, neutron powder diffraction patterns were recorded from $LaAlO_3$ in both the rhombohedral and cubic phases [20], but the focus of that work was thermal expansion rather than structure and the phase transition.

In summary, the occurrence of the $R\bar{3}c$ to $Pm\bar{3}m$ phase transition in $LaAlO_3$ is well established, and the general consensus [8, 14, 15, 18, 19] is that the transition temperature is in the vicinity of 800 K. Much less is known about the (presumed) analogous phase transitions in $PrAlO_3$ and $NdAlO_3$ because these occur, if at all, at higher temperatures and have rarely, if ever, been observed. Scott [18] estimated transition temperatures by extrapolation from the frequencies of selected Raman lines, and suggested transition temperatures for $PrAlO_3$ and $NdAlO_3$ as $1320 \pm 20$ and $1640 \pm 30$ K, respectively. Geller and Raccah [19], however, found that $PrAlO_3$ was still clearly rhombohedral at 1400 K. For their part, Geller and Raccah [19] located transitions in $La_{1-x}Pr_xAlO_3$ and $La_{1-x}Nd_xAlO_3$ and attempted to predict transition temperatures by linear extrapolation to $x = 1$. They suggested transitions at around 1640 and 2020 K for $PrAlO_3$ and $NdAlO_3$, respectively. One report [21] claims that the phase transition in $NdAlO_3$ occurs at 1400 K, but this is inconsistent with other observations, including those to be reported here—it seems likely this reflects the highest temperature at which the rhombohedral splitting in the x-ray diffraction pattern could be resolved. The present authors are unaware of any previous neutron diffraction study for $PrAlO_3$, though the room temperature structure has been determined using x-rays [22]. The room temperature structure of $NdAlO_3$ has been determined by both x-ray [23] and neutron [24] diffraction techniques.

In this paper we report neutron powder diffraction studies of $LaAlO_3$ from 20 K, through the phase transition, to 830 K, of $PrAlO_3$ from room temperature to 1763 K, and of $NdAlO_3$ from room temperature to 1673 K. Neutron diffraction has the advantage that the patterns are more sensitive to oxygen position than the corresponding x-ray patterns, so the oxygen position can be more accurately determined. This leads to good estimates of the oxygen atom octahedron rotation angle and strain, and our interest was to follow the temperature variation of these parameters, particularly as the phase transition is approached. Neutron diffraction

patterns recorded previously for $LaAlO_3$ at temperatures from 15 to 1230 K [20] have been reanalysed for inclusion with the present results.

## 2. Experimental procedure and data analysis

Polycrystalline samples of the three oxides $LnAlO_3$ (Ln = La, Pr, Nd) were prepared by heating stoichiometric mixtures of $Al(NO_3)_3{\cdot}9H_2O$ (Aldrich 98%) and the appropriate lanthanide salt, $La(ac)_3$ (Fluka AG 99%), $Pr_3O_4$ or $Nd_2O_3$ (Aldrich 99.9%) in an alumina crucible. The mixtures were successively heated at 700, 800 and 900 °C, for 24 h at each temperature, with re-grinding after each heating step. The samples were finally annealed, in air, at 1300°C (Ln = La), 1200 °C (Ln = Pr) or 1350 °C (Ln = Nd) for 72 h. Powder x-ray diffraction measurements, recorded on a Siemens D-5000 diffractometer using Cu K$\alpha$ radiation, confirmed the desired phases had been formed. The sample of $LaAlO_3$ investigated previously [20] was obtained by pulverizing single crystals grown by the flame-fusion method. Neutron diffraction data were collected using the HB-4 high-resolution powder diffractometer at the Oak Ridge National Laboratory. That diffractometer and the procedures employed have been described in detail in connection with the earlier study of $LaAlO_3$ [20]. For each of the compounds studied, about 10 g of powder were contained in a thin-walled, 13 mm diameter, vanadium sample can. Diffraction patterns were recorded, using neutrons of wavelength 1.500 Å, over the $2\theta$ range from 11 to 135°, with a step size of 0.05°. For the low temperature measurements of $LaAlO_3$, a closed-cycle helium refrigerator was used—for the measurements at room temperature and above, an ILL-type vacuum furnace was employed, the furnace being pumped to maintain a vacuum of about $10^{-6}$ Torr. Temperatures in the furnace were corrected according to the calibration described previously [20]. In each case, patterns were recorded at successively higher temperatures, to a maximum (in the case of $PrAlO_3$) of 1763 K. The crystal structures were refined by the Rietveld method, using the program LHPM [25] operating on a PC. The background was taken to be a quadratic function of $2\theta$, and was refined simultaneously with the unit-cell, zero-point, scale, peak width/shape/asymmetry and crystal structure parameters. The peak profile was described by a Voigt function, in which the widths of the Gaussian and Lorentzian components were coded to vary in accordance with the Caglioti *et al* function [26] to describe instrumental resolution and strain broadening, and with $\sec\theta$ to describe crystallite size broadening, respectively. The $2\theta$ region near 38°, affected by a peak from the furnace heating element, was excluded during the refinements.

## 3. Results

### *3.1. Lanthanum aluminate ($LaAlO_3$)*

In the present work, neutron diffraction patterns were recorded at a number of temperatures between 20 and 830 K, using smaller temperature intervals in the vicinity of the rhombohedral to cubic phase transition. Neutron diffraction patterns recorded in the course of the earlier study [20], at temperatures ranging from 15 to 1230 K, were also re-examined.

That $LaAlO_3$ is a rhombohedrally distorted perovskite at lower temperatures can be seen from a subtle splitting of the main peaks, attributed to distortion from the cubic metric, and additional weak peaks associated with the rotation of octahedra of oxygen atoms and the concomitant enlargement of the unit cell. The peak splitting is best resolved in our patterns (figure 1) at $2\theta$ about 87°, near the minimum of instrumental peak width, where what would be the 222 peak in cubic perovskite splits into the 404 and 0012 peaks in the rhombohedral phase. This splitting is well resolved only at the lowest temperatures, it results in asymmetry in the

peak at room temperature, and cannot be detected at higher temperatures. Better indicators of the rhombohedral phase are the weak 'superlattice' reflections, indicated by the arrows in figure 1. The most persistent of these as the transition to cubic is approached, are the 131 peak near 71°, the 333 at around 117° and the 511 in the vicinity of 127°. These peaks were still clearly observable at 803 K, and probably just observable at 812 K, but there was no suggestion of them in the pattern recorded at 830 K. Thus, the patterns recorded at temperatures up to 812 K were fitted assuming space group $R\bar{3}c$†, and those recorded at 830 K and higher assuming the ideal cubic structure. Further analysis (section 4) suggests that at 821 K the sample may be on the point of transition, where very small deviations from $Pm\bar{3}m$ probably cannot be observed. The 821 K pattern has therefore also been analysed as if cubic. Anisotropic atomic displacement parameters, appropriate to the different site symmetries, were refined in every case. The patterns recorded at 20 and 694 K, and the fits obtained, are shown in figure 1.

The results from all our refinements are given, in an abbreviated form, in table 1. The table shows the lattice parameter(s), and for refinements in space group $R\bar{3}c$, the oxygen $x$-parameter, which is the only variable position parameter in the structure. The lattice parameters, and their variation with temperature, are also shown in figure 2. A plot of $c/a$ in the hexagonal phase shows this ratio increasing monotonically with temperature towards $\sqrt{6} = 2.4495$ (its value in the cubic structure) up to 694 K, beyond which temperature it behaves erratically. When there is no observable splitting of the strongest Bragg reflection the hexagonal lattice parameters are sensitive to the positions of the weakening superlattice reflections and it is our view that these are unreliable at the higher temperatures. In figure 2 we include third order polynomial functions obtained by fitting the hexagonal lattice parameter results obtained at 694 K and below. A similar function has been used to describe the temperature variation of the lattice parameter in the cubic phase. The temperature variation of the $x$-parameter of the O atom, in space group $R\bar{3}c$, is shown in figure 3. We believe this parameter, being determined by the intensities of the weakening superlattice reflections, is better determined near the rhombohedral to cubic phase transition than the ratio of lattice parameters mentioned above. The $x$-parameter, and the octahedral rotation angle derived from it, are discussed in greater detail in section 4.

There is generally good agreement between our results and those from previous studies. For the lattice parameter comparisons, we examine the $c/a$ ratio, since, as just indicated, this ratio also provides a measure of the rhombohedral distortion. There is good agreement between our results at room temperature, $c/a = 2.4440$, (from table 1) and those from Geller and Raccah [19], $c/a = 2.4439$, from O'Bryan *et al* [8], $c/a = 2.442$, or from Taspinar and Cuneyt Tas [27], $c/a = 2.4440$. In addition, our value for the oxygen position parameter, $x(\mathrm{O}) = 0.5251(2)$, is in excellent agreement with that reported from the neutron diffraction of de Rango *et al* [12] which, in the setting used here, is $x(\mathrm{O}) = 1 - 0.475 = 0.525$. The comparison of the rotation angles derived from our results with those from the electron paramagnetic resonance study [15] is deferred to section 4.

### *3.2. Praseodymium aluminate ($PrAlO_3$)*

Neutron diffraction patterns from $PrAlO_3$ were recorded from room temperature to 1763 K, close to the maximum accessible temperature using the ILL-type furnace. The effects of rhombohedral distortion on the diffraction pattern are much less subtle than in the case of $LaAlO_3$, peak splitting being evident at temperatures of up to 1474 K. The superlattice peaks associated with octahedral rotation, indicated by the markers in figure 4, are again more

† The quality of the fits to the neutron diffraction patterns was such as to confirm the accepted space group as against a two phase alternative recently proposed [28].

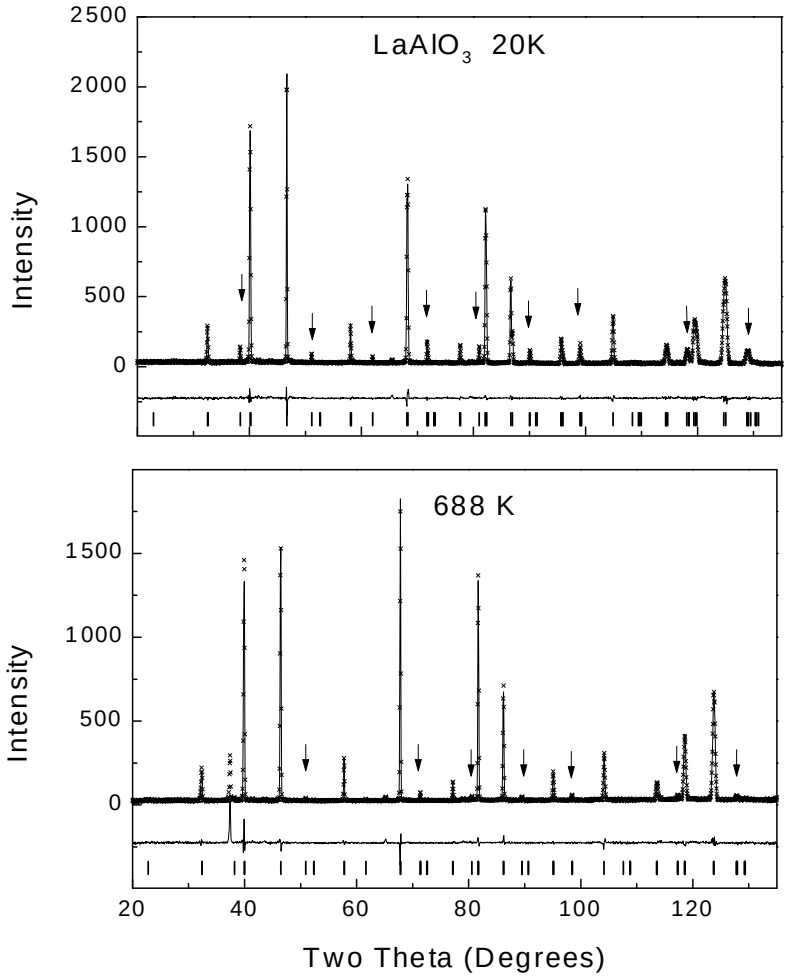


**Figure 1.** Neutron diffraction patterns ($\lambda = 1.500$ Å) obtained from $LaAlO_3$ at 20 and 694 K, with the results of fitting by the Rietveld method. The crosses are the observed data, the continuous curves through these are the patterns calculated after least-squares fitting, and the continuous trace under each pattern shows the difference between the observed and calculated patterns. Positions of Bragg peaks are indicated by the markers under the pattern. The peak near 38° is the 110 peak from the Nb heating element, and has been excluded from the analysis. The arrowed peaks are the superlattice peaks indicative of the rhombohedral phase. The measures of fit for the pattern at 20 K are $R_p = 6.7$, $R_{wp} = 9.1$ ($R_{exp} = 7.7$), $R_{Bragg} = 1.5\%$ and at 694 K, $R_p = 7.1$, $R_{wp} = 9.1$ ($R_{exp} = 8.0$), $R_{Bragg} = 1.6\%$.

persistent indicators of the rhombohedral symmetry. Though they continue to weaken as the temperature is increased and the phase transition approached, the strongest of these, the 131 peak, is still just discernible at 1763 K, the highest temperature attained. Thus all patterns were fitted assuming space group $R\bar{3}c$. The patterns recorded at room temperature and at 1733 K, and the fits obtained, are shown in figure 4. Abbreviated results from all measured temperatures are given in table 2.

The lattice parameters for $PrAlO_3$, and their variation with temperature, are shown in figure 5. A plot of $c/a$ shows erratic behaviour beyond 1673 K, so the lattice parameters recorded at higher temperatures are considered to be unreliable. Quadratic functions fitted to

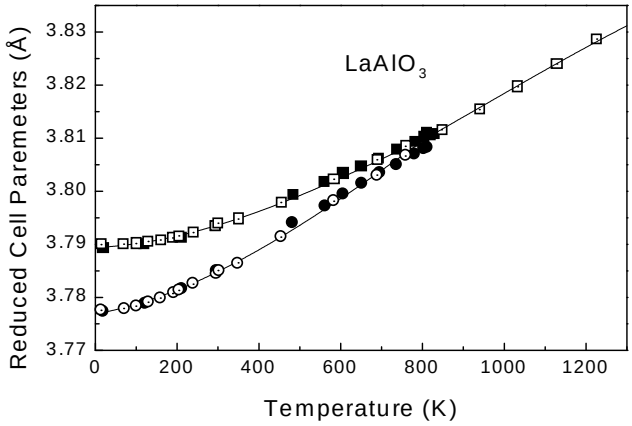


**Figure 2.** The temperature variation of the lattice parameters $a$ (■) and $c$ (●) of $LaAlO_3$ in the rhombohedral and cubic phases. The closed symbols are those data obtained in the present work and the open symbols from the reanalysis of the work in [20]. The parameters shown below the phase transition (820 K) are the reduced hexagonal lattice parameters $a/\sqrt{2}$ and $c/\sqrt{12}$, whereas above the phase transition the cubic lattice parameter $a$ is shown. This temperature variation is fitted by $a = 5.3590(1 + 9.0503 \times 10^{-7}\ T + 1.0657 \times 10^{-8}\ T^2 - 4.258 \times 10^{-12}\ T^3)$ Å and $c = 13.0836(1+3.5672\times10^{-6}\ T+1.3090\times10^{-8}\ T^2-5.1161\times10^{-12}\ T^3)$ Å in the rhombohedral phase, and by $a = 3.7849(1 + 2.6223 \times 10^{-6}\ T + 9.6488 \times 10^{-9}\ T^2 - 3.4083 \times 10^{-12}\ T^3)$ Å in the cubic phase.

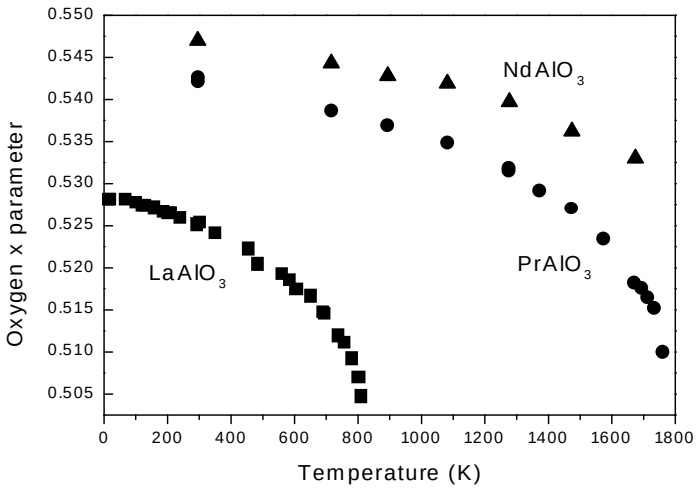


**Figure 3.** The temperature variation of the oxygen $x$-parameter in the rhombohedral phase for each of the compounds studied. Only in the case of $LaAlO_3$ was the cubic phase clearly attained.

the lattice parameter data up to and including the 1673 K point are included in the figure. The temperature variation of the $x$-parameter of the O atom is shown in figure 3. It appears the transition to cubic would occur a little above the highest temperature attained in this experiment, 1763 K, and certainly higher than the temperatures suggested previously [18, 19].

There is reasonable agreement between our results and those from the few previous studies. At room temperature we find $c/a = 2.4344$ compared with $c/a = 2.4327$ derived from Burbank [22], and $c/a = 2.4326$ from Geller and Raccah [19]. In the more conventional

**Table 1.** Cell parameter(s) for $LaAlO_3$, and the oxygen position parameter when in the rhombohedral space group, as a function of temperature. The table includes results obtained from reanalysis of patterns recorded previously by Chakoumakos *et al* [20]. The number in parentheses beside each entry indicates the esd in the last significant figure. In $R\bar{3}c$ the La occupies the 6a sites at $(00\frac{1}{4})$, the Al the 6b sites at (000) and the O the 18e sites at $(x0\frac{1}{4})$. In $Pm\bar{3}m$ the La occupies the 1b sites at $(\frac{1}{2}\frac{1}{2}\frac{1}{2})$, the Al the 1a sites at (000) and the O the 3d sites at $(\frac{1}{2}00)$.

| Temperature (K) | Patterns used | Space group | $a$ (Å) | $c$ (Å) | $x$ |
|---|---|---|---|---|---|
| 15[a] | Chakoumakos | $R\bar{3}c$ | 5.3598(1) | 13.0859(1) | 0.5281(1) |
| 20[a] | Present work | $R\bar{3}c$ | 5.3589(1) | 13.0858(3) | 0.5280(2) |
| 70[a] | Chakoumakos | $R\bar{3}c$ | 5.3599(1) | 13.0871(1) | 0.5280(1) |
| 100[a] | Chakoumakos | $R\bar{3}c$ | 5.3601(1) | 13.0886(1) | 0.5277(1) |
| 120[a] | Present work | $R\bar{3}c$ | 5.3598(1) | 13.0903(3) | 0.5274(2) |
| 130[a] | Chakoumakos | $R\bar{3}c$ | 5.3606(1) | 13.0911(1) | 0.5273(1) |
| 160[a] | Chakoumakos | $R\bar{3}c$ | 5.3610(1) | 13.0938(1) | 0.5271(1) |
| 190[a] | Chakoumakos | $R\bar{3}c$ | 5.3616(1) | 13.0969(2) | 0.5267(1) |
| 205[a] | Chakoumakos | $R\bar{3}c$ | 5.3621(1) | 13.0989(1) | 0.5264(1) |
| 210[a] | Present work | $R\bar{3}c$ | 5.3617(1) | 13.1000(3) | 0.5264(2) |
| 240[a] | Chakoumakos | $R\bar{3}c$ | 5.3630(1) | 13.1029(2) | 0.5259(1) |
| 295[a] | Chakoumakos | $R\bar{3}c$ | 5.3646(1) | 13.1095(2) | 0.5251(1) |
| 295 | Present work | $R\bar{3}c$ | 5.3647(1) | 13.1114(3) | 0.5251(2) |
| 301 | Chakoumakos | $R\bar{3}c$ | 5.3655(1) | 13.1119(3) | 0.5254(1) |
| 350[a] | Chakoumakos | $R\bar{3}c$ | 5.3666(1) | 13.1169(1) | 0.5241(1) |
| 455 | Chakoumakos | $R\bar{3}c$ | 5.3710(1) | 13.1336(3) | 0.5222(1) |
| 484 | Present work | $R\bar{3}c$ | 5.3730(1) | 13.1427(4) | 0.5204(2) |
| 561 | Present work | $R\bar{3}c$ | 5.3766(1) | 13.1539(4) | 0.5192(2) |
| 584 | Chakoumakos | $R\bar{3}c$ | 5.3772(1) | 13.1570(4) | 0.5185(2) |
| 607 | Present work | $R\bar{3}c$ | 5.3787(1) | 13.1617(5) | 0.5175(3) |
| 651 | Present work | $R\bar{3}c$ | 5.3807(1) | 13.1687(6) | 0.5166(3) |
| 690 | Chakoumakos | $R\bar{3}c$ | 5.3824(1) | 13.1741(6) | 0.5147(2) |
| 694 | Present work | $R\bar{3}c$ | 5.3827(2) | 13.1759(8) | 0.5145(3) |
| 738 | Present work | $R\bar{3}c$ | 5.3851(1) | 13.1808(7) | 0.5119(3) |
| 759 | Chakoumakos | $R\bar{3}c$ | 5.3860(2) | 13.1866(9) | 0.5111(3) |
| 781 | Present work | $R\bar{3}c$ | 5.3873(2) | 13.1876(8) | 0.5092(4) |
| 803 | Present work | $R\bar{3}c$ | 5.3884(2) | 13.1909(10) | 0.5069(5) |
| 812 | Present work | $R\bar{3}c$ | 5.3895(1) | 13.1919(8) | 0.5047(6) |
| 821 | Present work | $Pm\bar{3}m$ | 3.8106(1) | | |
| 830 | Present work | $Pm\bar{3}m$ | 3.8108(1) | | |
| 848 | Chakoumakos | $Pm\bar{3}m$ | 3.8116(1) | | |
| 940 | Chakoumakos | $Pm\bar{3}m$ | 3.8154(1) | | |
| 1034 | Chakoumakos | $Pm\bar{3}m$ | 3.8197(1) | | |
| 1130 | Chakoumakos | $Pm\bar{3}m$ | 3.8240(1) | | |
| 1227 | Chakoumakos | $Pm\bar{3}m$ | 3.8287(1) | | |

[a] These measurements were made with the sample in the closed cycle helium refrigerator. For other measurements, the sample was housed in the ILL-type furnace.

space group setting used here, the result from Burbank's x-ray study for the oxygen position is $x(\mathrm{O}) = 0.533$, compared with $x(\mathrm{O}) = 0.5421(2)$ obtained in the present neutron study.

### *3.3. Neodymium aluminate ($NdAlO_3$)*

Neutron diffraction patterns from $NdAlO_3$ were recorded at temperatures from room temperature to 1673 K. The effects of rhombohedral distortion on the diffraction pattern are

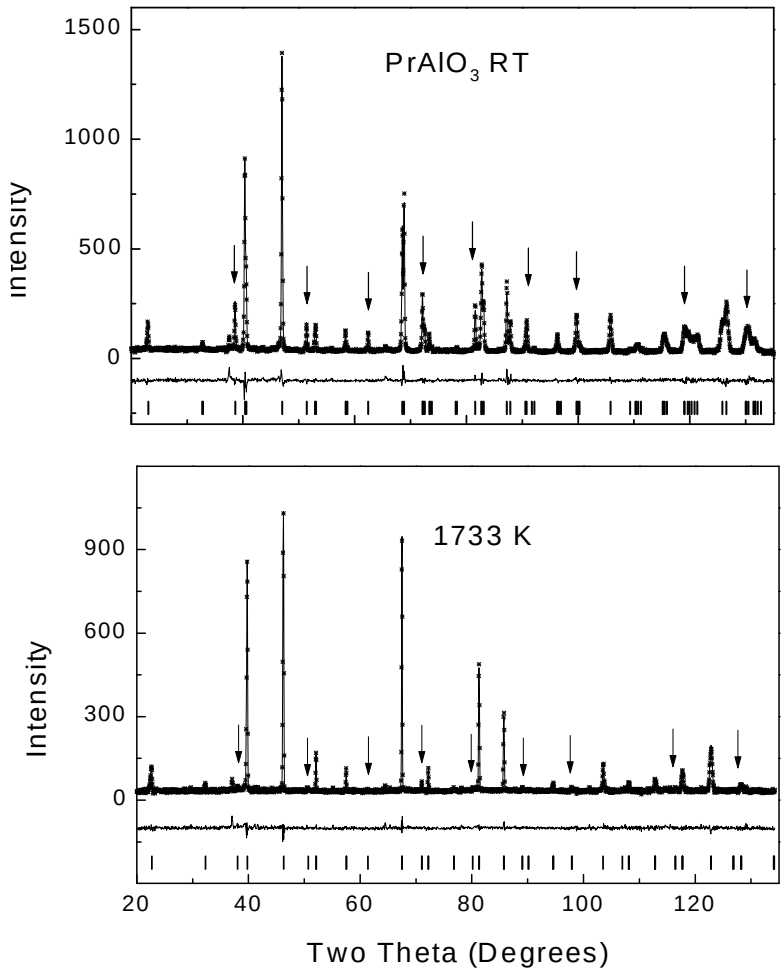


**Figure 4.** Neutron diffraction patterns ($\lambda = 1.500$ Å) obtained from $PrAlO_3$ at room temperature and at 1733 K, with the results of fitting by the Rietveld method. The data and fits are represented as in figure 1. The arrowed peaks are the superlattice peaks indicative of the rhombohedral phase. The measures of fit to the pattern at 295 K are $R_p = 7.1$, $R_{wp} = 8.9$ ($R_{exp} = 7.5$), $R_{Bragg} = 2.4\%$ and at 1733 K, $R_p = 7.2$, $R_{wp} = 9.0$ ($R_{exp} = 8.7$), $R_{Bragg} = 1.8\%$.

again obvious, in that several of the main peaks show splitting at room temperature (figure 6), and superlattice peaks associated with octahedral rotation, indicated by the markers in figure 6, are rather strong. The peak splitting is not so evident at higher temperatures, but the superlattice peaks are still clearly seen at 1673 K. All patterns were fitted assuming space group $R\bar{3}c$. The patterns recorded at room temperature and at 1673 K, and the fits obtained, are shown in figure 6. Abbreviated results from all measured temperatures are given in table 3.

The lattice parameters for $NdAlO_3$ vary smoothly with temperature, the temperature variation being well described by the quadratic functions $a = 5.3118(1 + 6.0613 \times 10^{-6}\ T + 1.6860 \times 10^{-9}\ T^2)$ Å and $c = 12.8846(1 + 1.1125 \times 10^{-5}\ T + 1.4612 \times 10^{-9}\ T^2)$ Å. The temperature variation of the $x$-parameter of the O atom is included in figure 3—it remains well above 0.5 (the value it would have in the cubic perovskite) at 1673 K, confirming the indication from the diffraction pattern that the transition to cubic is at a much higher temperature.

**Table 2.** Cell parameters and the oxygen position parameter for $PrAlO_3$, as a function of temperature. The space group is $R\bar{3}c$, with atomic coordinates as in table 1, even at the highest temperature attained.

| Temperature (K) | $a$ (Å) | $c$ (Å) | $x$ |
|---|---|---|---|
| 295 | 5.3337(2) | 12.9842(4) | 0.5421(2) |
| 295[a] | 5.3337(1) | 12.9766(4) | 0.5427(2) |
| 716 | 5.3504(2) | 13.0474(5) | 0.5387(2) |
| 894 | 5.3592(2) | 13.0784(5) | 0.5369(2) |
| 1082 | 5.3694(2) | 13.1128(5) | 0.5349(2) |
| 1277 | 5.3807(2) | 13.1486(5) | 0.5318(3) |
| 1277[a] | 5.3812(1) | 13.1510(3) | 0.5314(2) |
| 1375 | 5.3861(2) | 13.1676(6) | 0.5291(3) |
| 1474 | 5.3918(2) | 13.1871(7) | 0.5270(3) |
| 1574 | 5.3972(2) | 13.2035(7) | 0.5234(4) |
| 1673 | 5.4026(2) | 13.2239(12) | 0.5183(4) |
| 1695 | 5.4044(2) | 13.2271(11) | 0.5175(4) |
| 1713 | 5.4052(3) | 13.2335(17) | 0.5164(5) |
| 1733 | 5.4067(3) | 13.2360(15) | 0.5151(5) |
| 1763[a] | 5.4100(2) | 13.2443(17) | 0.5099(6) |

[a] These results were obtained from later measurements on the same sample.

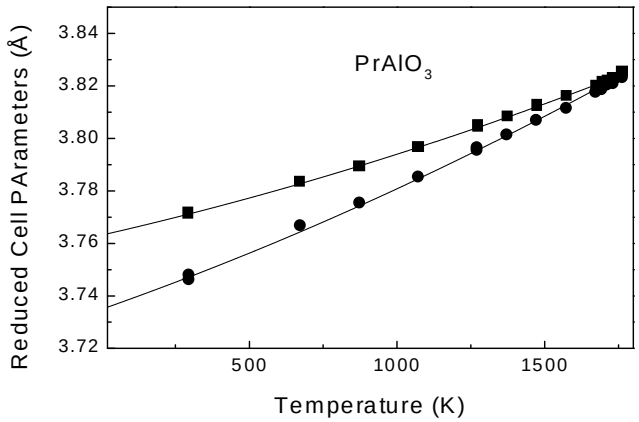


**Figure 5.** The temperature variation of the reduced lattice parameters, $a$ (■) and $c$ (●), of $PrAlO_3$ in the rhombohedral phase. This temperature variation is fitted by $a = 5.3219(1 + 6.8402 \times 10^{-6}\ T + 1.3518 \times 10^{-9}\ T^2)$ Å and $c = 12.9382(1 + 1.0602 \times 10^{-5}\ T + 1.6824 \times 10^{-9}\ T^2)$ Å.

Agreement between our results at room temperature and those from previous studies is good. For the lattice parameter ratios, we find $c/a = 2.4293$ compared with $c/a = 2.4283$ [19], $c/a = 2.4269$ [23] and $c/a = 2.4272$ [24] from previous x-ray and neutron studies. The value obtained here for the oxygen position parameter is $x(\mathrm{O}) = 0.5470(2)$, compared with $x(\mathrm{O}) = 0.5516(9)$ obtained using x-rays [23] and $x(\mathrm{O}) = 0.5477(2)$ using time-of-flight neutron powder diffraction [24].

## 4. Discussion

The main aim of this study was to examine the details of the rhombohedral to cubic transition in $R\bar{3}c$ perovskites. In the event, only in the case of $LaAlO_3$ could the sample be obtained in the

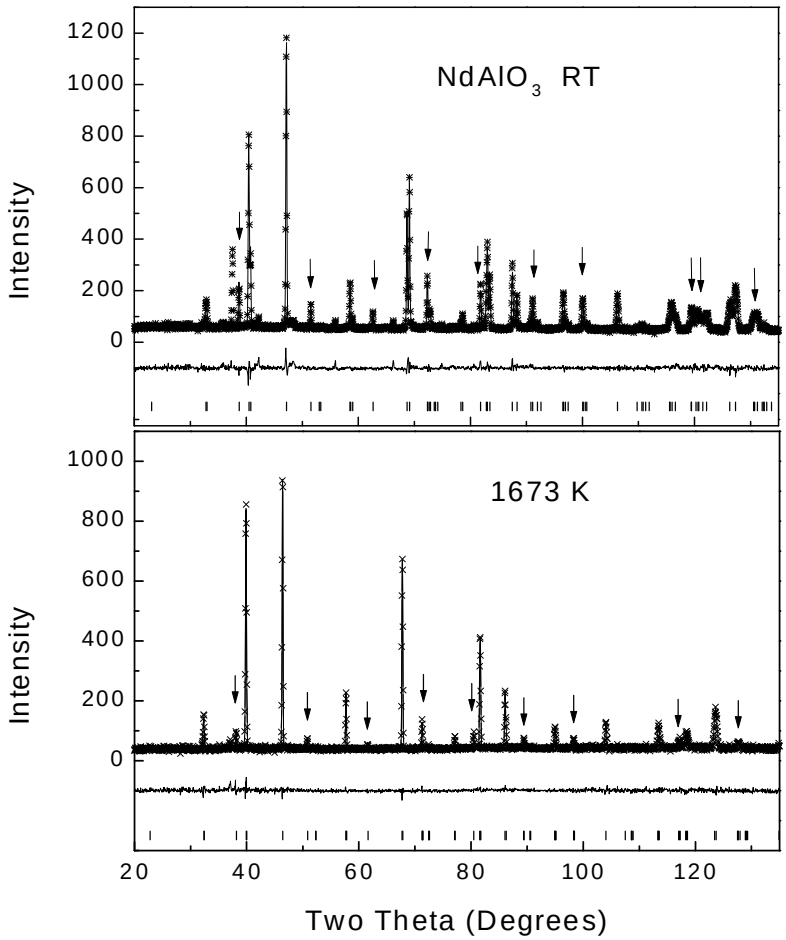


**Figure 6.** Neutron diffraction patterns ($\lambda = 1.500$ Å) obtained from $NdAlO_3$ at room temperature and at 1673 K, with the results of fitting by the Rietveld method. The data and fits are represented as in figures 1 and 4. The measures of fit to the pattern at 295 K are $R_p = 6.4$, $R_{wp} = 8.2$ ($R_{exp} = 6.7$), $R_{Bragg} = 2.4\%$ and at 1673 K, $R_p = 6.5$, $R_{wp} = 7.9$ ($R_{exp} = 8.0$), $R_{Bragg} = 1.6\%$.

cubic phase, although in the case of $PrAlO_3$ the close approach to the transition could be studied. However, with the added data on $NdAlO_3$ presented here, data from $LaGaO_3$ from our own previous study [5], and results from previous studies of the rhombohedral perovskites $LaCoO_3$ [29] and $LaNiO_3$ [30], the body of experimental data on these rhombohedral perovskites is now substantial.

### *4.1. Rhombohedral distortion*

As mentioned earlier, the difference of the lattice parameter ratio $c/(a\sqrt{6})$ from unity is a measure of the rhombohedral distortion. An equivalent measure is the difference from 60° of the angle $\alpha$ of the primitive rhombohedral cell†. The values at room temperature (whenever possible) of these quantities for the different rhombohedral $R\bar{3}c$ perovskites are collected in table 4.

† The connection between these quantities is given, for example, by equation 10.43 of Megaw [31].

**Table 3.** Cell parameters and the oxygen position parameter for $NdAlO_3$, as a function of temperature. The space group is $R\bar{3}c$, with atomic coordinates as in table 1.

| Temperature (K) | $a$ (Å) | $c$ (Å) | $x$ |
|---|---|---|---|
| 295 | 5.3223(2) | 12.9292(5) | 0.5470(2) |
| 716 | 5.3391(2) | 12.9958(4) | 0.5443(2) |
| 894 | 5.3471(2) | 13.0262(5) | 0.5428(3) |
| 1082 | 5.3573(2) | 13.0626(6) | 0.5419(3) |
| 1277 | 5.3677(2) | 13.0989(6) | 0.5397(3) |
| 1474 | 5.3796(2) | 13.1386(5) | 0.5362(4) |
| 1673 | 5.3902(2) | 13.1756(5) | 0.5330(4) |

**Table 4.** Measures of rhombohedral distortion in $R\bar{3}c$ perovskites. The entries for $c/(a\sqrt{6})$ and $\alpha$ correspond to descriptions on the hexagonal and primitive rhombohedral cells, respectively.

| Compound | Temperature | $c/(a\sqrt{6})$ | $\alpha$ (°) | Reference |
|---|---|---|---|---|
| $LaAlO_3$ | Room | 0.9978 | 60.10 | Table 1 |
| $PrAlO_3$ | Room | 0.9938 | 60.27 | Table 2 |
| $NdAlO_3$ | Room | 0.9917 | 60.37 | Table 3 |
| $BaTbO_3$ | Room | 0.9917 | 60.37 | Jacobson *et al* [32] |
| $LaGaO_3$ | 673 K | 0.9894 | 60.47 | Howard and Kennedy [5] |
| $LaGaO_3$ | Room (by extrapolation) | 0.9868 | 60.59 | Howard and Kennedy [5] |
| $LaMnO_3$ | 350 K | 0.9847 | 60.68 | Huang *et al* [33] |
| $LaNiO_3$ | Room | 0.9834 | 60.74 | Garcia-Munoz *et al* [30] |
| $LaCoO_3$ | Room | 0.9821 | 60.80 | Thornton *et al* [29] |

The entries are made in order of increasing rhombohedral distortion, and certain qualitative conclusions can be drawn about the systematics. The transition to the cubic phase, expected in principle in all of these perovskites, occurs at around 800 K in $LaAlO_3$ (the least distorted at room temperature), and at around 1800 K in $PrAlO_3$ (the next least distorted). In no other case has the transition been observed or approached. It seems likely that the greater the rhombohedral distortion at room temperature, the higher the temperature of the transition to cubic. On the other hand, there appears to be no correlation between the degree of distortion at room temperature and the low temperature behaviour of these perovskites; $LaAlO_3$ (this and earlier work), $LaNiO_3$ [30] and $LaCoO_3$ [29] are known to retain the rhombohedral structures to helium temperatures, whereas $PrAlO_3$ undergoes two phase transition below room temperature [22], and $LaGaO_3$ is in fact orthorhombic at room temperature [5]. The situation for $BaTbO_3$ at low temperatures is unclear [34, 35]. The rhombohedral distortion is associated with octahedral tilting (for details see next paragraph), and this in turn is an adaptation of the ideal perovskite structure to accommodate undersized cations in the A sites [31]. Comparing the three rare-earth aluminates studied here, the rhombohedral distortion increases in the sequence (of A site cations) $La^{3+}$, $Pr^{3+}$, $Nd^{3+}$, in order of decreasing ionic radii. Alternatively, comparing the La compounds, the rhombohedral distortion increases in the sequence (of B site cations) $Al^{3+}$, $Ga^{3+}$, in order of increasing ionic radii. These two subsets of the rhombohedral $R\bar{3}c$ perovskites evidently show the expected trends, however, more complex behaviour is observed when a transition metal ion (Mn, Co or Ni) is on the B site.

### *4.2. Octahedral rotation and strain*

The rhombohedral distortion in the $R\bar{3}c$ perovskites is a result of the rotation and strain of oxygen atom octahedra. The relations of the octahedral rotation angle and strain parameter

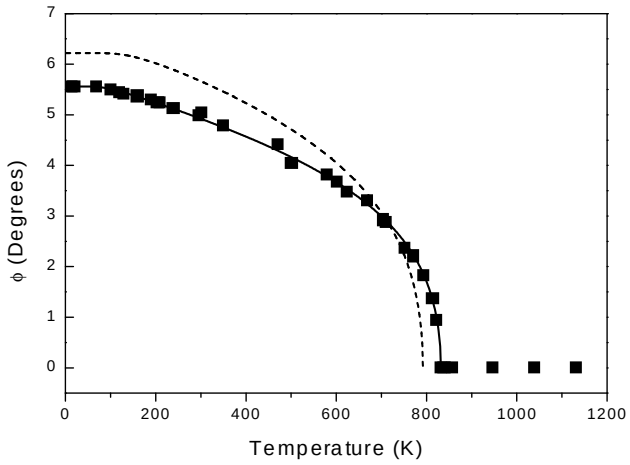


**Figure 7.** The temperature variation of the octahedral rotation angle in $LaAlO_3$. The points represent the values derived from the oxygen $x$-parameter (using equation (1)), and the continuous curve through these points is obtained from equation (5) (see text). The dashed curve represents the results obtained by Müller *et al* [15] using electron paramagnetic resonance techniques.

to the lattice parameters and oxygen $x$-parameter have been presented previously [5, 36]. To summarize, in the setting of $R\bar{3}c$ we have used, the angle of rotation $\phi$ of the octahedron (away from its orientation in the cubic perovskite) is given by

$$\tan\phi = 2u\sqrt{3} \tag{1}$$

where $u = x(\mathrm{O}) - \frac{1}{2}$. The strain parameter $\eta$, ($\eta > 1$, $\eta = 1$, $\eta < 1$ accordingly as the octahedron is elongated in the direction parallel to the threefold axis, regular, or compressed along this axis) is given by

$$\eta = \frac{c\cos\phi}{a\sqrt{6}}. \tag{2}$$

Equation (1) was used to convert the oxygen $x$-parameter to the rotation angle $\phi$, then equation (2) was employed to evaluate the strain $\eta$ from $\phi$, $c$ and $a$. In general, the rotation angle decreases as the temperature increases, and the octahedra are compressed along the threefold axis, but become more regular as the temperature is increased. The octahedral rotation and the octahedral strain are, in the rhombohedral structure, two geometrically independent parameters. Nevertheless, they are likely to be coupled, and the nature of this coupling (especially in the vicinity of the rhombohedral to cubic phase transition) is of interest.

### *4.3. Lanthanum aluminate (*$LaAlO_3$*)*

This is the compound on which we have the greatest number of results, and represents the only case in which we followed the transition into the cubic phase. The temperature variation of the octahedral rotation angle is shown in figure 7, along with results for the same octahedral rotation angle obtained by electron paramagnetic resonance measurements on $Fe^{3+}$ doped $LaAlO_3$ [15]. The agreement is generally pleasing, though there are minor discrepancies in the temperature variation and a relatively small, unexplained, difference of about $0.5^\circ$ in the estimates of octahedral rotation angle at the lowest temperatures.

The temperature variation of the octahedral strain, calculated from equation (2), is shown in figure 8. Given the uncertainty in lattice parameters in the vicinity of the phase transition, noted

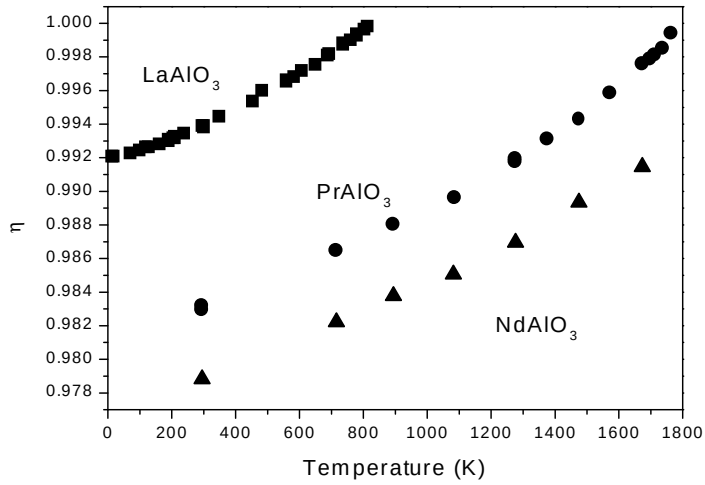


**Figure 8.** The temperature variation of the octahedral strain, $\eta$, in the rhombohedral phase, for each of the compounds studied.

in section 3.1, the calculations are based on lattice parameters obtained from the previously fitted polynomials, along with the experimentally determined values of the rotation angle $\phi$. Based on these estimates, the octahedral strain parameter increases smoothly (though not linearly) towards unity as the phase transition is approached. The question of coupling between octahedral strain and rotation angle has been considered previously by Megaw and Darlington [36], who suggested the strain might depend on the square of the rotation angle:

$$1 - \eta \propto \phi^2. \tag{3}$$

In our earlier study of $LaGaO_3$ [5], remote from the phase transition, we were led to doubt a coupling of this form. By contrast, in the present case of $LaAlO_3$ (and based on using fitted rather than measured lattice parameters), by plotting $1 - \eta$ versus $\phi^2$ (figure 9) we find that (3) gives a good description of the coupling near the phase transition, and in fact provides an adequate description over the entire temperature range.

The octahedral rotation angle can be taken to represent the order parameter, and as such we sought a function to fit its temperature variation. A reasonable fit in the vicinity of the transition, that is above about 600 K, can be obtained with a quadratic, of the form

$$\phi = A(T_c - T)^{1/2} \tag{4}$$

where $T_c$ is the transition temperature and $A$ a constant. Such variation is indicative of a continuous, second order phase transition [37]. The fit provided by equation (4) is, however, poor at lower temperatures. For this reason we have attempted to fit the data using $\phi(T) = \zeta(T)\phi(0)$, where $\phi(0)$ is the angle of rotation at 0 K, and $\zeta(T)$ is the solution of

$$\zeta = \tanh[\zeta(1 + g\zeta^2 + h\zeta^4)T_c/T]. \tag{5}$$

This corresponds to a generalized mean field treatment of the phase transition [38–40]. Mathematically, the variation in $\zeta(T)$ (and hence in $\phi$) can be continuous only for $g \leqslant 1/3$. For $g < 1/3$ the leading term in the expansion just below $T_c$ is of the form $\phi \propto (T_c - T)^{1/2}$, corresponding to a second order phase transition. To obtain a continuous variation with $g = 1/3$ it is also necessary that $h \leqslant 1/5$, in which case the leading term in the expansion is of the form $\phi \propto (T_c - T)^{1/4}$, corresponding to a transition of tricritical type [37]. The function $\zeta(T)$ shows

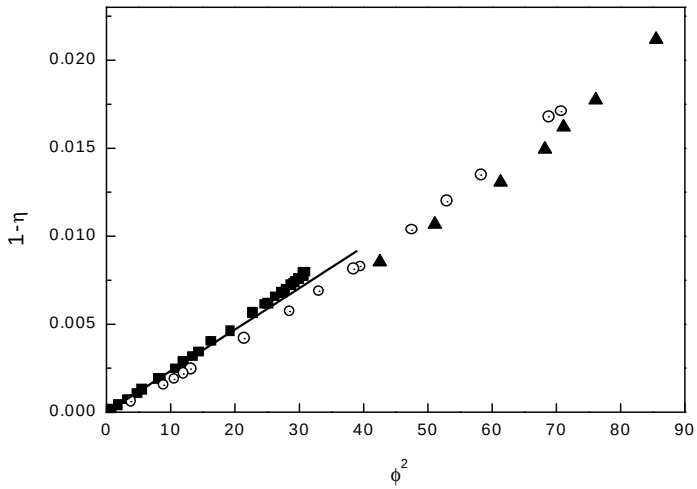


**Figure 9.** The variation of $1-\eta$ with $\phi^2$ in the rhombohedral phase, for $LaAlO_3$ (■) $PrAlO_3$ (○) and $NdAlO_3$ (▲). The line corresponds to $1-\eta = 0.72\phi^2$ ($\phi$ in rad) and represents a straight line fit to the $LaAlO_3$ data near the origin.

saturation behaviour at low temperatures, giving better agreement with the observations. We have successfully fitted our data with a function of this kind (figure 7), with the parameters $\phi(0) = 5.6^\circ$, $T_c = 820$ K, $g = 0$, $h = -0.70$. This is consistent with the suggestion that the transition is second order in nature. We note that the results from Müller *et al* [15] can be fitted with a similar function, with parameters $\phi(0) = 6.2^\circ$, $T_c = 792$ K, $g = 0$, $h = -0.53$.

### *4.4. Praseodymium aluminate ($PrAlO_3$)*

In $PrAlO_3$ the structural evolution of the rhombohedral phase was followed to near the phase transition to cubic, the experiment stopping due to the failure of the sample holder at these high temperatures, an estimated 5 K below the transition temperature. The temperature variation of the octahedral rotation angle is shown in figure 10. This variation is again well described by the application of the mean field result, equation (5), the parameters in this case being $\phi(0) = 8.5^\circ$, $T_c = 1768$ K, $g = 1/3$, $h = -0.95$. In $PrAlO_3$, therefore, the rhombohedral to cubic phase transition appears to be of tricritical type. The temperature variation of the octahedral strain, calculated as explained in section 4.3, is shown in figure 8. Again, the octahedral strain parameter increases smoothly towards unity as the phase transition is approached. The coupling between octahedral strain and rotation angle is well described by (3) near the phase transition (see figure 9), though the coupling deviates significantly from such a relationship away from the transition.

### *4.5. Neodymium aluminate ($NdAlO_3$)*

In the case of $NdAlO_3$, as for $LaGaO_3$, which was the subject of our previous study [5], it became apparent that even at the maximum accessible temperature, we would still be far below the temperature of the transition to the cubic phase. Accordingly, the measurements on this compound were stopped at 1673 K. The octahedral rotation was derived as before, and its temperature variation is shown in figure 10. The temperature variation of the octahedral strain, and its relationship to the rotation angle, are indicated in figures 8 and 9, respectively.

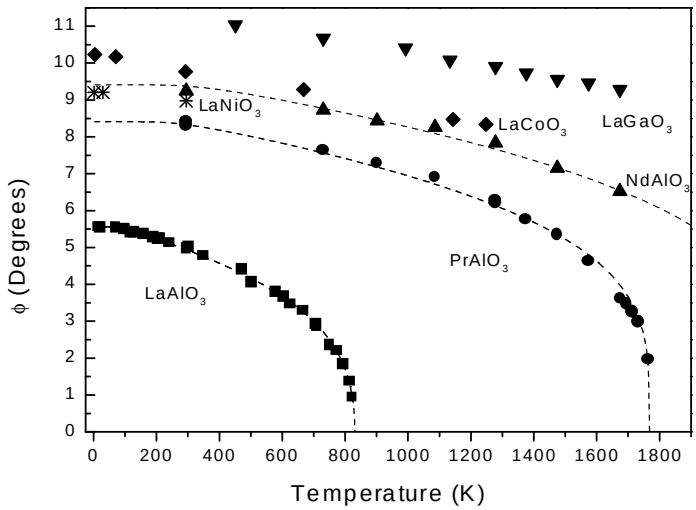


**Figure 10.** The temperature variation of the octahedral rotation angle, derived from the oxygen position as measured by neutron diffraction, in six rhombohedral $R\bar{3}c$ perovskites. The results on the rare-earth aluminates are from the present study, whereas the results on $LaNiO_3$, $LaCoO_3$ and $LaGaO_3$ have been taken or derived from previously published work [5, 29, 30]. The dashed curves shown fitting the results are obtained by the application of a generalized mean field theory, as explained in the text.

We believe there is little to gain from any detailed discussion of the functional form of the temperature variations, nor the strain–rotation coupling, at temperatures which we believe to be some hundreds of degrees below the phase transition. Nevertheless, a rough fit of a function similar to that used in the case of $PrAlO_3$, suggests that the zero temperature rotation angle is about $9.4^\circ$ and the transition temperature about 2180 K.

### *4.6. Systematic trends and summary*

We have completed structural studies of the rhombohedral ($R\bar{3}c$) rare-earth aluminates, $LaAlO_3$, $PrAlO_3$ and $NdAlO_3$, with particular reference to the rotation and strain of the oxygen octahedra, and the transition or approach to the cubic phase. When data from our own previous study on $LaGaO_3$ [5], and from other neutron diffraction studies of the rhombohedral perovskites $LaCoO_3$ [29] and $LaNiO_3$ [30] are added, an examination of the systematics is possible. Measurements have been made at more than one temperature in every case.

It may not yet be possible to predict whether an arbitrary perovskite, $ABO_3$, forms a rhombohedral structure, but systematics are evident in series in which either A or B remains unchanged. As indicated in section 4.1, the rhombohedral distortion increases in sequences in which either the A site cation decreases in radius or the B site cation increases in radius. A greater degree of misfit may lead to a more complex (e.g. orthorhombic) distortion, e.g., when in $BaTbO_3$ the Ba ion is replaced by the smaller Sr ion or the Tb ion [35] by the larger Pr ion [32] an orthorhombic perovskite results.

From the neutron diffraction data, octahedral rotation angles can be calculated†, and these are displayed as a function of temperature for the six compounds for which such data are

† In calculating the rotation angle for $LaCoO_3$, we have made the assumption that the lattice parameter at 1248 K shown in [29] as 5.150(2) Å should read 5.510(2) Å.

available (figure 10). In every case, the rotation angle diminishes as the temperature increases, suggesting an approach towards the cubic phase. Only in the case of $LaAlO_3$ has the transition to cubic actually been observed, although in $PrAlO_3$ it seems that the transition was closely approached. The trend of the data suggests that the transition temperature would be higher for compounds with larger initial rotation angles, and though the data on this are extremely limited we conjecture that the transition temperature (if the sample were to survive to the transition) might vary roughly as the square of the low temperature rotation angle. The temperature variations of the rotation angles in $LaAlO_3$ and $PrAlO_3$ have been successfully fitted by the application of a generalized mean field theory, as explained in sections 4.3 and 4.4. This analysis indicates that the transition in $LaAlO_3$ is a second order transition, whereas that in $PrAlO_3$ is of a tricritical type. The reason for this difference (along with differences between the natures of the transitions in $SrZrO_3$ and $SrHfO_3$ [3, 6]) is not yet understood.

The variation of the octahedral strain with temperature for the rare-earth aluminates studied here is shown in figure 8. The coupling of the strain to the rotation angle is of greater interest here, and this is illustrated in figure 9. It is clear that for $LaAlO_3$ and $PrAlO_3$ near the phase transition, the coupling is well described by the proportionality (3), $1 - \eta \propto \phi^2$, although higher powers of $\phi$ are needed to describe the coupling further from the transition. The initial slope of the $1 - \eta$ versus $\phi^2$ plot is smaller in the case of $PrAlO_3$ than in the case of $LaAlO_3$, and (extrapolating towards the expected phase transition) smaller again in the case of $NdAlO_3$. In short, the idea [36] that strain–rotation coupling follows $1 - \eta \propto \phi^2$ is vindicated in the vicinity of the phase transition, but the constant of proportionality is not universal. The temperature dependence of the strain is implied by its coupling to the rotation and the temperature dependence of the rotation angle—specifically, near the transition for a second order transition we would have $1-\eta \propto T_c-T$ and for a tricritical transition $1-\eta \propto (T_c-T)^{1/2}$.

It is unfortunate that for most of the $R\bar{3}c$ perovskites the rhombohedral to cubic phase transition remains inaccessible. This is especially the case since it is of interest to understand the nature of the phase transition, including determining how the transition temperature correlates with the low temperature octahedral rotation angle. A limitation of the present work has been the difficulty in determining the $c/a$ ratio close to the phase transition, and a high resolution study of perovskites with mixed site occupancies, such as $La_{1-x}Pr_xAlO_3$, where the transition temperature should depend on the extent of substitution, would be worthwhile.

## Acknowledgments

The authors thank A K Prodjosantoso for the preparation of the samples. Financial support from the Access to Major Research Facilities Program is gratefully acknowledged. Oak Ridge National Laboratory is managed by Lockheed Martin Energy Research Corporation for the US Department of Energy under contract No DE-AC05-96OR22464.

## References

[1] Kennedy B J and Hunter B A 1998 *Phys. Rev.* B **58** 653
[2] Howard C J and Stokes H T 1998 *Acta Crystallogr.* B **54** 782
[3] Kennedy B J, Howard C J and Chakoumakos B C 1999 *Phys. Rev.* B **59** 4023
[4] Kennedy B J, Howard C J and Chakoumakos B C 1999 *J. Phys.: Condens. Matter* **11** 1479
[5] Howard C J and Kennedy B J 1999 *J. Phys.: Condens. Matter* **11** 3229
[6] Kennedy B J, Howard C J and Chakoumakos B C 1999 *Phys. Rev.* B **60** 2972
[7] Kennedy B J, Prodjosantoso A K and Howard C J 1999 *J. Phys.: Condens. Matter* **11** 3229
[8] O'Bryan H M, Gallagher P K, Berkstresser G W and Brandle C D 1990 *J. Mater. Res.* **5** 183
[9] Marti W, Fischer P, Altorfer F, Scheel H J and Tadin M 1994 *J. Phys.: Condens. Matter* **6** 127

[10] Marti W, Fischer P, Schefer J and Kubel F 1996 *Z. Kristallogr.* **211** 891
[11] Geller S and Bala V B 1956 *Acta Crystallogr.* **9** 1019
[12] de Rango C, Tsoucaris G and Zelwer C 1964 *C.R. Acad. Sci. Paris* **259** 1537
[13] Derighetti B, Drumheller J E, Laves F, Müller K A and Waldner F 1965 *Acta Crystallogr.* **18** 557
[14] Fay H and Brandle C D 1967 *J. Appl. Phys.* **38** 3405
[15] Müller K A, Berlinger W and Waldner F 1968 *Phys. Rev. Lett.* **21** 814
[16] Cochran W and Zia A 1968 *Phys. Status Solidi* **25** 273
[17] Axe J D, Shirane G and Müller K A *Bull. Am. Phys. Soc.* **14** 61
[18] Scott J F 1969 *Phys. Rev.* B **183** 823
[19] Geller S and Raccah P M 1970 *Phys. Rev.* B **2** 1167
[20] Chakoumakos B C, Schlom D G, Urbanik M and Luine J 1998 *J. Appl. Phys.* **83** 1979
[21] Masao M, Yamada T and Tetsuo N 1977 *Yogyo Kyokai Shi* **85** 90
[22] Burbank R D 1970 *J. Appl. Crystallogr.* **3** 112
[23] Marezio M, Dernier P and Remeika P 1972 *J. Sol. State Chem.* **4** 11
[24] Roult G, Pastuszak R, Marchand R and Laurent Y 1983 *Acta Crystallogr.* C **39** 673
[25] Hill R J and Howard C J 1986 *Australian Atomic Energy Commission* (now ANSTO) *Report* M112
[26] Caglioti G, Paoletti A and Ricci F P 1958 *Nucl. Instrum.* **3** 223
[27] Taspinar E and Cuneyt Tas A 1997 *J. Am. Ceram. Soc.* **80** 133
[28] Yang C Y, Huang Z R, Yang W H, Zhou Y Q and Fung K K 1991 *Acta Crystallogr.* A **47** 703
[29] Thornton G, Tofield B C and Hewat A W 1986 *J. Sol. State Chem.* **61** 301
[30] Garcia-Munoz J L, Rodriguez-Carvajal J, Lacorre P and Torrance J B 1992 *Phys. Rev.* B **46** 4414
[31] Megaw H D 1973 *Crystal Structures: A Working Approach* (Philadelphia, PA: Saunders)
[32] Jacobson A J, Tofield B C and Fender B E F 1972 *Acta Crystallogr.* B **28** 956
[33] Huang Q, Santoro A, Lynn J W, Erwin R W, Borchers J A, Peng J L and Greene R L1997 *Phys. Rev.* B **55** 14 987
[34] Banks E, LaPlaca S J, Kunnmann W, Corliss L M and Hastings J M 1972 *Acta Crystallogr.* B **28** 3429
[35] Tezuka K, Hinatsu Y, Shimojo Y and Morii Y 1998 *J. Phys.: Condens. Matter* **10** 11 703
[36] Megaw H D and Darlington C N W 1975 *Acta Crystallogr.* A **31** 161
[37] Salje E K H 1990 *Phase Transitions in Ferroelastic and Co-elastic Crystals* (Cambridge: Cambridge University Press)
[38] Lifante G, Gonzalo J A and Windsch W W 1993 *Ferroelectics* **146** 107
[39] Noheda B, Cereceda N, Iglesias T, Lifante G, Gonzalo J A, Chen T and Wang Y 1995 *Phys. Rev.* B **51** 16 388
[40] Cereceda N, Noheda B, Iglesias T, Fernandez-del-Castillo J R, Gonzalo J A, Duan N, Wang Y L, Cox D E and Shirane G 1997 *Phys. Rev.* B **55** 6174